A 2-Stage Para-Hermitian Eigenvalue Decomposition for Crowd Counting in an Indoor Setting Based on the Scattered Radio Field

Frank E. Ebong
Institute of Networked and Embedded Systems
University of Klagenfurt, Klagenfurt, Austria
frank.ebong@aau.at

Andrea M. Tonello
Institute of Networked and Embedded Systems
University of Klagenfurt, Klagenfurt, Austria
andrea.tonello@aau.at

***Abstract*—In this paper, we propose a Sliding Window 2-Stage Para-Hermitian Eigenvalue Decomposition (PhEVD) algorithm for extracting the scattering amplitudes of a scattered radio field from a high-dimensional and multichannel, time-varying Wi-Fi Channel State Information (CSI) data in a multi-antenna setup. The algorithm is designed to address the computational challenges associated with processing large, high-dimensional and multichannel Wi-Fi CSI data. We evaluate the proposed method on real-world Wi-Fi Channel State Information (CSI) data collected in an indoor environment, considering seven distinct scenarios ranging from an empty room to a room with up to six people. The extracted scattering amplitudes are used to classify these scenarios using a fine-tuned Gaussian Support Vector Machine (SVM). Our experimental results demonstrate that the proposed 2-Stage PhEVD algorithm outperforms state-of-the-art feature extraction methods, such as Reconstruction Independent Component Analysis (RICA) and sparse filtering, in terms of classification accuracy of the scattered radio field. This work highlights the potential of the proposed approach for device-free sensing, non-intrusive crowd counting and other applications in indoor sensing.**

***Index Terms*—PhEVD, scattering amplitude, scattered radio field , channel frequency response.**

I. Introduction

The rapid advancement of wireless communication technologies has opened new avenues for non-contact sensing applications [1], particularly in indoor environments. Among these, indoor crowd counting [2] and analytics have emerged as critical tasks for various applications, including security, retail, and smart building management. Traditional methods for crowd counting often rely on cameras, which can be intrusive and raise privacy concerns. In contrast, device-free sensing using Wi-Fi signals offers a non-intrusive and privacy-preserving alternative. By leveraging the pervasiveness of Wi-Fi infrastructure, it is possible to infer the presence and movement of people within an environment based on human-induced scattering of these Wi-Fi radio waves.

Contribution. This paper presents a novel approach for indoor crowd counting by analyzing the scattering amplitudes of the scattered radio field, captured through high-dimensional and multichannel time-varying Wi-Fi Channel State Information (CSI) data, considering a multi-antenna setup. We propose a two-stage Para-Hermitian Eigenvalue Decomposition (PhEVD) algorithm, termed the Sliding Window 2-Stage PhEVD, to extract the scattering amplitudes of the radio field. The algorithm is specifically designed to address the computational challenges associated with processing large-scale, multichannel Wi-Fi radio signals.

The proposed method is tested on real-world data collected from a bistatic Wi-Fi-based sensing system in an indoor environment. Seven different scenarios are considered, ranging from an empty room to a room with up to six people. The scattering amplitudes extracted by the 2-Stage PhEVD are then used to classify these scenarios using a fine-tuned Gaussian Support Vector Machine (SVM). The performance of our algorithm is compared against state-of-the-art feature extraction algorithms.

The remainder of this paper is organized as follows: Section II introduces the signal and system model, detailing the propagation of Wi-Fi signals in an indoor environment with static and dynamic paths. Section III describes the Sliding Window 2-Stage PhEVD algorithm, including its mathematical formulation and computational advantages. Section IV presents the experimental setup and results, highlighting the accuracy of the proposed method in crowd counting. Finally, Section V concludes the paper, summarizing the key contributions and potential applications of the proposed approach.

Notation. The set of natural, real, and complex-valued numbers are denoted by $\mathbb{N}$, $\mathbb{R}$, and $\mathbb{C}$ respectively. Additionally, scalars are denoted as italic letters ($H, \dots, \alpha, \Gamma, \dots$), column vectors as lower-case bold-face letters ($\mathbf{d}, \mathbf{v}, , \dots$), matrices as bold-face capitals ($\mathbf{H}, \mathbf{G}, \dots$), and tensors are written as bold-face calligraphic letters ($\boldsymbol{\mathcal{D}}, \boldsymbol{\mathcal{H}}, \dots$). Furthermore, $(\cdot)^\dagger$ represents the Hermitian transpose, and $diag(\cdot)$ extracts the diagonal elements of a matrix.

II. Signal and System Model

Consider the bistatic Wi-Fi-based non-contact sensing system shown in Fig. 1, where the radio signals transmitted by a Wi-Fi transmitter arrive at a separate Wi-Fi receiver through multiple paths induced by scattering from objects and human targets in the indoor environment.

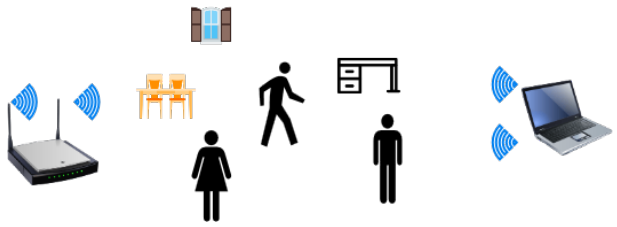

Fig. 1. Scenario of human targets and inanimate objects in an environment scattering Wi-Fi radio waves.

Now, consider a broadband Wi-Fi signal that propagates through a static path such as the Line-of-sight (LoS) path from transmitter to receiver. The single tone transmitted signal can be written as $X(f,t) = \alpha(t)e^{j2\pi ft}$ at time t for every frequency f [3]. Likewise, the receive signal through the static path is given by $Y(f,t) = \alpha'(t)e^{j2\pi f(t-\tau_s)}$, where $\tau_s = l_s/c$ is the time delay on the static path of length l_s, $\alpha'(t)$ is the attenuation signal. The transfer function of this static path is given by

$$H_s(f,t) = \frac{Y(f,t)}{X(f,t)} = \frac{\alpha'(t)e^{j2\pi f(t-\tau_s)}}{\alpha(t)e^{j2\pi ft}} = \Gamma(t)e^{-j2\pi f\tau_s},\ \forall\ f \tag{1}$$

where $\Gamma(t) = \alpha'(t)/\alpha(t)$ is the amplitude of the transfer function. For moving human targets in the indoor environment, there is a frequent perturbation of the radio field, this causes regular changes in the reflected and diffracted paths, creating a dynamic path [3]. The received signal through the dynamic path is given by $Y_d(f,t) = \alpha''(t)e^{j2\pi(f+f_D)(t-\tau_d)}$, for all f, where τ_d is the time delay on the dynamic path and f_D is the Doppler frequency shift [3] with $f_D \ll f$. The transfer function for the dynamic path is given by

$$\begin{aligned} H_d(f,t) &= \frac{Y_d(f,t)}{X(f,t)} = \frac{\alpha''(t)e^{j2\pi(f+f_D)(t-\tau_d)}}{\alpha(t)e^{j2\pi ft}} \\ &\cong \Gamma'(t)e^{j2\pi(f_Dt-f\tau_d)},\ \forall\ f, \end{aligned} \tag{2}$$

where $\Gamma'(t) = \alpha''(t)/\alpha(t)$.

Hence, for a given bistatic scenario, the overall transfer function or channel frequency response is given by

$$\begin{aligned} H(f,t) = &\sum_{m\in P_S} \Gamma_m(t)e^{-j2\pi f\tau_s^{(m)}} \\ &+\sum_{n\in P_D} \Gamma'_n(t)e^{j2\pi(f_{Dn}t-f\tau_d^{(n)})},\ \forall\ f \end{aligned} \tag{3}$$

where P_s is the set of static paths and P_D is the set of dynamic paths.

For a multi-antenna system, (3) is the transfer function or channel response between a transmit and a receive antenna pair. Therefore, assuming N_T transmit antennas and N_R receive antennas, we have that

$$\begin{aligned} H_{a,b}(f,t) = &\sum_{m\in P_S} \Gamma_m(t)e^{-j2\pi f\tau_s^{(m)}} \\ &+\sum_{n\in P_D} \Gamma'_n(t)e^{j2\pi(f_{Dn}t-f\tau_d^{(n)})},\ \forall\ f \end{aligned}$$

with $a \in \{1,\dots,N_T\}$ and $b \in \{1,\dots,N_R\}$. Thus, for the multi-antenna system, we have that

$$\mathbf{H}(f,t) = \begin{bmatrix} H_{1,1}(f,t) & \cdots & H_{1,N_R}(f,t) \\ H_{2,1}(f,t) & \cdots & H_{2,N_R}(f,t) \\ \vdots & \vdots & \vdots \\ H_{N_T,1}(f,t) & \cdots & H_{N_T,N_R}(f,t) \end{bmatrix}, \tag{4}$$

where $\mathbf{H}(f,t) \in \mathbb{C}^{N_T\times N_R},\ \forall\ f$.

III. The Sliding Window 2-Stage Para-Hermitian Eigenvalue Decomposition (PhEVD)

Analysis of the scattered radio field across a range of frequencies, using high-dimensional and multichannel Wi-Fi radio signals from a multi-antenna system, can prove to be particularly important in applications such as *crowd analytics* and *crowd counting*. This is crucial for deriving actionable insights, such as estimating crowd density, while operating in a *device-free* and *non-intrusive* manner.

However, processing high-dimensional and multichannel Wi-Fi radio signals from a multi-antenna system can pose a significant computational burden on many numerical computing frameworks. This is especially true when mathematical operations are applied to these Wi-Fi signals to extract important features of the scattered radio field. In many cases, these operations can cause the systems on which they are executed to slow down or even crash.

Therefore, in this section, we describe our algorithm, called the Sliding Window 2-Stage Para-Hermitian Eigenvalue Decomposition (PhEVD). This algorithm aids in analyzing the scattered radio field across a range of frequencies at a given time. Additionally, it significantly reduces the computational burden on numerical computing frameworks.

It is worth noting that this algorithm works for the special case where $N_T = N_R$.

A. Algorithm Description

Given $0 \le t \le \Upsilon$, the algorithm starts by time sloting the time window into time slots of duration Δt, for all $H_{a,b}(f,t)$ at a given frequency f_k. Here, $k = [1,\dots,K]$, where $k \in \mathbb{N}$ corresponds to the index of a given Wi-Fi sub-channel or frequency bin. Thus, we can write $t = i\Delta t + l\Upsilon s$, where Υs is the sampling time, $l \in \{0,\dots L-1\}$ is the number of samples in a given time slot, and $i \in \mathbb{N}$, $i = [1,\dots,I]$, indicates the time slot number. Hence, the corresponding transfer function for an arbitrary transmit and receive antenna pair can be written as $H_{a,b}^{(i)}(f_k, l\Upsilon s) \in \mathbb{C}^L$. Next, a Toeplitzification operator [4] $\mathbf{T}_L$ to collect all samples over time in a matrix,

is applied to $H_{a,b}^{(i)}(f_k, l\Upsilon s)$ to embed it into the space $\mathbb{T}_L$ of Toeplitz matrices of $\mathbb{C}^{L\times L}$, i.e.,

$$\mathbf{T}_L : \begin{cases} \mathbb{C}^L \to \mathbb{T}_L \subset \mathbb{C}^{L\times L} \\ H_{a,b}^{(i)}(f_k, l\Upsilon s) \mapsto \mathbf{T}_L\left(H_{a,b}^{(i)}(f_k, l\Upsilon s)\right) := \mathbf{H}_{a,b}^{(i)}(f_k) \end{cases} \tag{5}$$

where $\mathbf{H}_{a,b}^{(i)}(f_k) \in \mathbb{C}^{L\times L}$ is the resulting Toeplitz matrix. Applying the Toeplitzification operator to all frequency bins or sub-channels, i.e., $\{f_k\}_{k=1}^K$, for a given time slot of index i, we obtain the tensor $\boldsymbol{\mathcal{H}}_{a,b}^{(i)} \in \mathbb{C}^{L\times L\times K}$, for all antenna pairs.

The algorithm proceeds by taking the PhEVD [5] of all the different combinations of transmit-receive antenna pairs $\boldsymbol{\mathcal{H}}_{a,b}^{(i)}$. The PhEVD which we shall be describing is obtained via successive finite impulse response para-unitary (FIR PU) transforms [6]. We start by defining $\mathbf{G}(e^{j2\pi f})$ an $L\times L$ causal FIR PU system of McMillan degree R [7], given by

$$\mathbf{G}(e^{j2\pi f}) = \left(\prod_{r=1}^{R} \mathbf{V}_r(e^{j2\pi f})\right) \mathbf{Q}(e^{j2\pi f}) \tag{7}$$

where $\mathbf{V}_r(e^{j2\pi f})$ is a degree-1 building block given by [6] [7]

$$\mathbf{V}_r(e^{j2\pi f}) = \mathbf{I}_L - \mathbf{v}_r\mathbf{v}_r^\dagger + e^{-j2\pi f}\mathbf{v}_r\mathbf{v}_r^\dagger, \quad 1 \le r \le R \tag{8}$$

where $\mathbf{I}_L$ is $L \times L$ identity matrix, $\mathbf{v}_r$ are $L \times 1$ unit vectors, and $\mathbf{Q} \in \mathbb{C}^{L\times L}$ is a Para-unitary matrix, i.e., $\mathbf{Q}^\dagger(e^{j2\pi f})\mathbf{Q}(e^{j2\pi f}) = \mathbf{I}_L$. Hence, $\mathbf{G}^\dagger(e^{j2\pi f})\mathbf{G}(e^{j2\pi f}) = \mathbf{I}_L$. Applying the degree-1 FIR PU transformation to $\boldsymbol{\mathcal{H}}_{a,b}^{(i)}$ we obtain

$$\boldsymbol{\mathcal{D}}_{a,b}^{(i)} \triangleq \boldsymbol{\mathcal{G}}^\dagger\boldsymbol{\mathcal{H}}_{a,b}^{(i)}\boldsymbol{\mathcal{G}} = \boldsymbol{\mathcal{Q}}^\dagger\left(\boldsymbol{\mathcal{V}}^\dagger\boldsymbol{\mathcal{H}}_{a,b}^{(i)}\boldsymbol{\mathcal{V}}\right)\boldsymbol{\mathcal{Q}}, \tag{9}$$

where (9) is done $\forall\ f$, and $\boldsymbol{\mathcal{G}} \in \mathbb{C}^{L\times L\times K}$, $\boldsymbol{\mathcal{Q}} \in \mathbb{C}^{L\times L\times K}$, $\boldsymbol{\mathcal{V}} \in \mathbb{R}^{L\times L\times K}$ are the tensors of $\mathbf{G}$, $\mathbf{Q}$ and $\mathbf{V}$ respectively. Here, (9) describes the transformation of the original system $\boldsymbol{\mathcal{H}}_{a,b}^{(i)}$ into a new system $\boldsymbol{\mathcal{D}}_{a,b}^{(i)}$ using $\boldsymbol{\mathcal{G}}$. The goal is to diagonalize $\boldsymbol{\mathcal{H}}_{a,b}^{(i)}$ by iteratively applying FIR PU transformations, increasing the Zeroth-Order Diagonal Energy (ZODE) [6] of all $\boldsymbol{\mathcal{H}}_{a,b}^{(i)}$. From (9), we define

$$\boldsymbol{\mathcal{P}}_{a,b}^{(i)} \triangleq \boldsymbol{\mathcal{V}}^\dagger\boldsymbol{\mathcal{H}}^{(i)}\boldsymbol{\mathcal{V}}. \tag{10}$$

Additionally, we define the zeroth-order term [6] of $\boldsymbol{\mathcal{H}}_{a,b}^{(i)}$ as

$$\mathbf{H}_{a,b}^{(i)}(f_0) = \int_1^K \boldsymbol{\mathcal{H}}_{a,b}^{(i)}\, df \tag{11}$$

where $\mathbf{H}_{a,b}^{(i)}(f_0) \in \mathbb{C}^{L\times L}$. Therefore, we define the zeroth-order diagonal energy (ZODE) to be be the energy of the diagonal components of the zeroth order term, expressed as

$$\Lambda_{\mathbf{H}_{a,b}} = \left\| diag\left(\mathbf{H}_{a,b}^{(i)}(f_0)\right)\right\|_2^2. \tag{12}$$

We can say that the zeroth-order term represents the average behavior of the scattered radio field across all frequencies and captures the dominant energy of the scattered radio field. To increase the Zeroth-Order Diagonal Energy (ZODE), we choose the vector $\mathbf{v}$ from the set of canonical basis vectors (unit element vectors) in the L-dimensional vector space. This choice ensures that $\mathbf{v}$ collects energy into the zeroth-order term. Subsequently, the tensor $\boldsymbol{\mathcal{Q}}$ is used to diagonalize the zeroth-order term, redistributing the energy along the diagonal elements.

The algorithm describes the iterative diagonalization of all the entries of $\boldsymbol{\mathcal{H}}_{a,b}^{(i)}$, and consequently, the ZODE of the scattered radio field is progressively maximized. Below is the step-by-step description of the algorithm.

Algorithm 1 Iterative diagonalization of $\boldsymbol{\mathcal{H}}_{a,b}^{(i)}$

Require: $\boldsymbol{\mathcal{H}}_{a,b}^{(i)}$
Ensure: $\boldsymbol{\mathcal{D}}_{a,b}^{(i)}$
Initialization:
$\boldsymbol{\mathcal{D}}_{a,b(0)}^{(i)} \leftarrow \boldsymbol{\mathcal{Q}}_0^\dagger\boldsymbol{\mathcal{H}}_{a,b}^{(i)}\boldsymbol{\mathcal{Q}}_0$
$r \leftarrow 1$
Iterative diagonalization:
while $r \le R$ **do**
  Step 1: Compute $\mathbf{V}_r(e^{j2\pi f})$
  $\mathbf{V}_r(e^{j2\pi f}) \leftarrow \mathbf{I}_L - \mathbf{v}_r\mathbf{v}_r^\dagger + e^{-j2\pi f}\mathbf{v}_r\mathbf{v}_r^\dagger$
  Construct the tensor $\boldsymbol{\mathcal{V}}$ **from the matrices** $\mathbf{V}_r(e^{j2\pi f_k})$ **for** $f = f_k$ **and** $k = 1, \ldots, K$
  Step 2: Apply transformation
  $\boldsymbol{\mathcal{P}}_{a,b(r)}^{(i)} \leftarrow \boldsymbol{\mathcal{V}}_r^\dagger\boldsymbol{\mathcal{H}}_{a,b(r-1)}^{(i)}\boldsymbol{\mathcal{V}}_r$
  Step 3: Diagonalize transformed system,
  $\boldsymbol{\mathcal{D}}_{a,b(r)}^{(i)} \leftarrow \boldsymbol{\mathcal{Q}}_r^\dagger\boldsymbol{\mathcal{P}}_{a,b(r)}^{(i)}\boldsymbol{\mathcal{Q}}_r$
  $r \leftarrow r + 1$
end while
Return:
return $\boldsymbol{\mathcal{D}}_{a,b(R)}^{(i)}$

In the initialization phase of Algorithm 1, $\mathbf{Q}_0(e^{j2\pi f})$ is obtained such that

$$\mathbf{D}_{a,b(0)}^{(i)}(e^{j2\pi f_0}) = \mathbf{Q}_0^\dagger(e^{j2\pi f_0})\mathbf{H}_{a,b}^{(i)}(f_0)\mathbf{Q}_0(e^{j2\pi f_0}).$$

Subsequently, $\mathbf{Q}_r(e^{j2\pi f_0})$ is computed from

$$\mathbf{D}_{a,b(r)}^{(i)}(e^{j2\pi f_0}) = \mathbf{Q}_r^\dagger(e^{j2\pi f_0})\mathbf{P}_{a,b(r)}^{(i)}(e^{j2\pi f_0})\mathbf{Q}_r(e^{j2\pi f_0}).$$

Hence, $\mathbf{D}_{a,b(r)}^{(i)}(e^{j2\pi f_0})$ can be made diagonal by choosing $\mathbf{Q}_r(e^{j2\pi f_0})$ to be matrix of eigenvectors of $\mathbf{H}_{a,b}^{(i)}(f_0)$ for $r = 0$ and $\mathbf{P}_{a,b(r)}^{(i)}(e^{j2\pi f_0})$ for $1 \le r \le R$. After performing the first stage of the PhEVD algorithm, we obtain

$$\boldsymbol{\mathcal{D}}^{(i)} = \begin{bmatrix} \boldsymbol{\mathcal{D}}_{1,1}^{(i)} & \cdots & \boldsymbol{\mathcal{D}}_{1,LN_R}^{(i)} \\ \boldsymbol{\mathcal{D}}_{2,1}^{(i)} & \cdots & \boldsymbol{\mathcal{D}}_{2,LN_R}^{(i)} \\ \vdots & \vdots & \vdots \\ \boldsymbol{\mathcal{D}}_{LN_T,1}^{(i)} & \cdots & \boldsymbol{\mathcal{D}}_{LN_T,LN_R}^{(i)} \end{bmatrix} \tag{13}$$

where $\boldsymbol{\mathcal{D}}^{(i)} \in \mathbb{C}^{LN_T \times LN_R \times K}$. In the second stage, we first select only the highest eigenvalues of all the the $\boldsymbol{\mathcal{D}}_{a,b}^{(i)}$ such we obtain $\tilde{\boldsymbol{\mathcal{D}}}^{(i)} \in \mathbb{C}^{N_T \times N_R \times K}$. Next, we take the cross spectral density of $\tilde{\boldsymbol{\mathcal{D}}}^{(i)}$ given by

$$\boldsymbol{\mathcal{B}}^{(i)} = \tilde{\boldsymbol{\mathcal{D}}}^{\dagger(i)} \tilde{\boldsymbol{\mathcal{D}}}^{(i)}, \tag{14}$$

where $\boldsymbol{\mathcal{B}}^{(i)} \in \mathbb{C}^{N_T \times N_R \times K}$. Similarly to stage 1, we iteratively diagonalize $\boldsymbol{\mathcal{B}}^{(i)}$ using algorithm 1, and again extract only the most dominant eigenvalue, which we denote with $\mathbf{d}^{(i)} \in \mathbb{R}^{K \times 1}$. The algorithm describing the second stage of the proposed PhEVD algorithm is given below

Algorithm 2 Extraction of the scattering amplitudes across all frequencies

Require: $\boldsymbol{\mathcal{D}}^{(i)} \in \mathbb{C}^{LN_T \times LN_R \times K}$ ▷ Input tensor
Ensure: $\mathbf{d} \in \mathbb{R}^{K \times 1}$ ▷ Most dominant eigenvalues across frequencies
1: **Step 1: Select Highest Eigenvalues**
2: $\tilde{\boldsymbol{\mathcal{D}}}^{(i)} \in \mathbb{C}^{N_T \times N_R \times K} \leftarrow$ SelectHighestEigenvalues$(\boldsymbol{\mathcal{D}}^{(i)})$ ▷ Extract highest eigenvalues
3: **Step 2: Compute Cross Spectral Density**
4: $\boldsymbol{\mathcal{B}}^{(i)} \leftarrow \tilde{\boldsymbol{\mathcal{D}}}^{\dagger(i)} \tilde{\boldsymbol{\mathcal{D}}}^{(i)}$ ▷ Compute cross spectral density
5: **Step 3: Diagonalize and Extract Dominant Eigenvalues**
6: Apply Algorithm 1 to $\boldsymbol{\mathcal{B}}^{(i)}$ ▷ Iteratively diagonalize
7: $\mathbf{d} \leftarrow$ ExtractMostDominantEigenvalues$(\boldsymbol{\mathcal{B}}^{(i)})$ ▷ Extract most dominant eigenvalues
8: **Return:**
9: **return** $\mathbf{d}^{(i)} \in \mathbb{R}^{K \times 1}$ ▷ Return dominant eigenvalue

The extracted $\mathbf{d}^{(i)}$ describes the scattering amplitude of the Wi-Fi radio signal over all frequencies for a given time slot i. The 2-stage PhEVD is performed for all time slots of the different transmit-receive antenna pairs, and the scattering amplitudes are arranged in the matrix $\mathbf{S}_\sigma = [\mathbf{d}_\sigma^{(1)}, \ldots, \mathbf{d}_\sigma^{(I)}]$. Here, $\mathbf{S}_\sigma \in \mathbb{R}^{K \times I}$, and $\sigma \in \mathbb{N}$ indicates the label of the scenario we are dealing with. For instance, $\sigma = 0$ corresponds to an empty room scenario, and $\sigma = 4$ corresponds to a scenario with 4 people in the room.

B. Classification of the scattering amplitudes extracted using the 2-stage PhEVD

The final phase of the algorithm consists in applying a classifier to the radio wave scattering amplitudes stored in the matrix $\mathbf{S}_\sigma = [\mathbf{d}_\sigma^{(1)}, \ldots, \mathbf{d}_\sigma^{(I)}]$, for crowd analytics in an indoor environment, such as counting the number of people in a given indoor setting. The classifier chosen in this paper is a fine-tuned Gaussian Support Vector Machine (SVM), also known as a Radial Basis Function (RBF) kernel SVM.

For better understanding, in Section IV, we report the extracted scattering amplitude of a given time slot for 7 indoor scenarios, ranging from an empty room to a room with up to 6 people, using our proposed algorithm.

IV. Experimental Results

In our experiment, we utilized two AX200 Wi-Fi network interface cards (NICs) to collect Channel State Information (CSI) from scattered Wi-Fi radio signals in a room measuring $3 \times 5.6 \times 7.3\ m^3$. One NIC was configured as a transmitter and the other as a receiver, with each card equipped with two omnidirectional antennas, forming a 2×2 MIMO (Multiple-Input Multiple-Output) system with each antenna elevated 1.5 meters above ground level. The Wi-Fi signal operated at a center frequency of 5.775 GHz with a bandwidth of 80 MHz, utilizing 245 sub-channels under the IEEE 802.11ac standard. CSI data was collected using Picoscenes at a sampling frequency of 80 MHz. The experiment comprised seven distinct scenarios. The initial scenario involved an indoor environment with no human presence. Subsequent scenarios introduced one to six individuals, with the primary activity being walking to enhance the scattered radio field. For each scenario, measurements were conducted over a duration of five minutes, yielding 5000 CSI samples for each sub-channel and each transmit-receive antenna pair. To facilitate analysis, the 5000 CSI samples were divided into 10 time slots (corresponding to $I = 10$), each containing 500 CSI samples (equivalent to $\Delta t \approx 30\ s$, and $\Upsilon \approx 60\ ms$). This time slotation was applied to each sub-channel and transmit-receive antenna pair. Our proposed 2-stage PhEVD algorithm, as described in Section III.A, was then applied to extract the scattering amplitudes for each scenario. The scattering amplitudes of the Wi-Fi radio signal over all 245 frequencies (Wi-Fi sub channels) of the system for $i = 5$, for 7 scenarios, i.e., empty room, and one person to 6 people in the room is shown in Fig. 2.

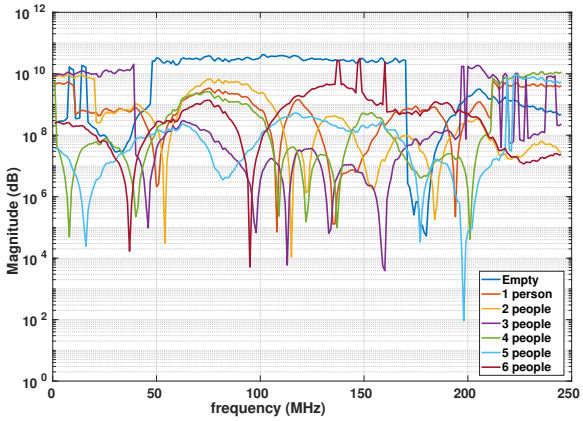

Fig. 2. Scattering Amplitude over all frequencies ($\{f_k\}_{k=1}^{245}$) for $i = 5$, and for 7 scenarios.

In Fig. 2, it can be observed that the scattering amplitudes extracted using the 2-stage PhEVD for the 7 scenarios—ranging from an empty room to a room with 1 to 6 people—each exhibit a distinct spectral signature. To corroborate this observation, the RBF kernel SVM classifier was applied to the scattering amplitudes extracted by the 2-stage PhEVD algorithm for all time slots, with the goal of people counting

in an indoor environment. The accuracy of our proposed algorithm was compared against two state-of-the-art feature extraction methods: Reconstruction Independent Component Analysis (RICA) [8] and sparse filtering [9], both applied to the same high-dimensional and multichannel CSI data, as reported in Table I. It can be seen from the table that the 2-stage PhEVD performs the best in distinguishing the scenarios in the indoor environment based on the scattered radio field.

It is worth mentioning that RICA and sparse filtering are considered state-of-the-art for small to medium-sized datasets, as in our case. If the number of samples had been significantly larger, we could have also considered using Artificial Neural Networks for feature extraction [10] and as a replacement for the RBF Kernel SVM [11].

TABLE I
COMPARISON OF PRE-PROCESSING ALGORITHMS FOR HUMAN TARGET COUNTING IN AN INDOOR SETTING USING RBF KERNEL SVM AS A CLASSIFIER.

Pre-Processing Algorithm	**Accuracy (%)**
No processing	60.9
Sparse filtering [9]	66.6
RICA [8]	69.9
2-Stage PhEVD (this paper)	90.2

Moreover, the confusion matrix obtained for the RBF kernel SVM applied to the scattering amplitudes obtained using the 2-stage PhEVD is shown in Fig. 3.

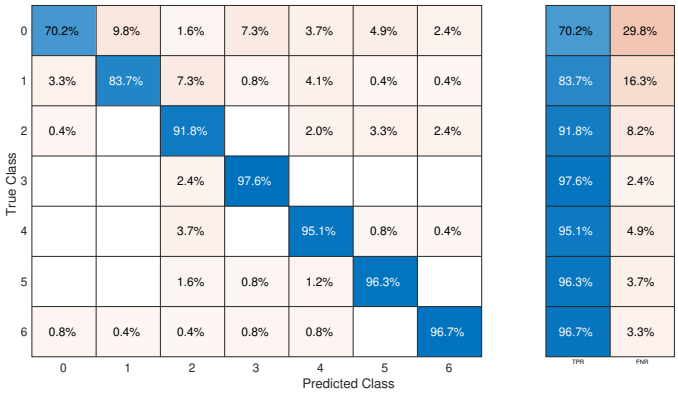

Fig. 3. Confusion matrix for the 2-stage PhEVD, with TPR=True Positive Rates, and FNR=False Negative Rates, the empty spaces are 0%.

The confusion matrix demonstrates that the scattering amplitudes extracted using the 2-Stage PhEVD algorithm is particularly effective for the classifier in distinguishing between an empty room and rooms with people, and it also performs well in identifying the correct number of people in most cases. However, from the confusion matrix, it can be observed that the True Positive Rate (TPR) for the empty room is the lowest among all scenarios. The TPR of 70.2% for the empty room can be explained by the fact that inanimate objects (such as furniture, walls, doors, and other static structures) cause static scattering of the Wi-Fi signals. This static scattering contributes to the total scattered field, creating a baseline level of signal perturbation even when no people are present. When people are introduced into the room, their movements cause dynamic scattering, which is superimposed on the static scattering from inanimate objects. This poses a little challenge for the classifier to distinguish the empty room from other scenarios.

V. CONCLUSION

In this paper, we have shown that by using the sliding window 2-stage PhEVD, we can extract the scattering amplitude of a radio scattered field from high-dimensional and multichannel Channel State Information (CSI) data, for a multi-antenna setup. Additionally, the extracted scattering amplitudes can be used in applications such as crowd analytics. For future work, we intend to apply this approach to different indoor environments of varying complexities.

REFERENCES

[1] N. Novello and A. M. Tonello, "Recurrent dqn for radio fingerprinting with constrained measurements collection," *ICT Express*, 2024.

[2] F. E. Ebong, N. Novello, and A. M. Tonello, "Human detection based on learning and classification of radio scattering parameters and para-hermitian eigenvalue decomposition," in *2024 IEEE 35th International Symposium on Personal, Indoor and Mobile Radio Communications (PIMRC)*, pp. 1–6, 2024.

[3] K. Niu, X. Wang, F. Zhang, R. Zheng, Z. Yao, and D. Zhang, "Rethinking doppler effect for accurate velocity estimation with commodity wifi devices," *IEEE Journal on Selected Areas in Communications*, vol. 40, no. 7, pp. 2164–2178, 2022.

[4] M. Simeoni, A. Besson, P. Hurley, and M. Vetterli, "Cpgd: Cadzow plug-and-play gradient descent for generalised fri," *IEEE Transactions on Signal Processing*, vol. 69, pp. 42–57, 2021.

[5] S. Weiss, J. Pestana, and I. K. Proudler, "On the existence and uniqueness of the eigenvalue decomposition of a parahermitian matrix," *IEEE Transactions on Signal Processing*, vol. 66, no. 10, pp. 2659–2672, 2018.

[6] A. Tkacenko, "Approximate eigenvalue decomposition of para-hermitian systems through successive fir paraunitary transformations," in *2010 IEEE International Conference on Acoustics, Speech and Signal Processing*, pp. 4074–4077, IEEE, 2010.

[7] P. Vaidyanathan, *Multirate filter banks and wavelets*. Prentice Hall, 1992.

[8] Q. Le, A. Karpenko, J. Ngiam, and A. Ng, "Ica with reconstruction cost for efficient overcomplete feature learning," *Advances in neural information processing systems*, vol. 24, 2011.

[9] J. Ngiam, Z. Chen, S. Bhaskar, P. Koh, and A. Ng, "Sparse filtering," *Advances in neural information processing systems*, vol. 24, 2011.

[10] Y. Chen, H. Jiang, C. Li, X. Jia, and P. Ghamisi, "Deep feature extraction and classification of hyperspectral images based on convolutional neural networks," *IEEE transactions on geoscience and remote sensing*, vol. 54, no. 10, pp. 6232–6251, 2016.

[11] N. Novello and A. M. Tonello, "f-divergence based classification: Beyond the use of cross-entropy," in *Proceedings of the 41st International Conference on Machine Learning*, pp. 38448–38473, PMLR, 2024.